THE JOURNAL OF BIOLOGICAL CHEMISTRY
Vol. 280, No. 18, Issue of May 6, pp. 17953–17960, 2005

Printed in U.S.A.

The Importance of Dynamic Effects on the Enzyme Activity

X-RAY STRUCTURE AND MOLECULAR DYNAMICS OF ONCONASE MUTANTS*

Received for publication, February 4, 2005
Published, JBC Papers in Press, February 22, 2005, DOI 10.1074/jbc.M501339200

Antonello Merlino‡§, Lelio Mazzarella‡§¶‖, Anna Carannante‡, Anna Di Fiore‡, Alberto Di Donato, Eugenio Notomista**, and Filomena Sica‡§¶‡‡**

*From the ‡Dipartimento di Chimica, Università degli Studi di Napoli "Federico II," Via Cynthia, 80126 Napoli, §Centro Regionale di Competenza-Bioteknet, Complesso Ristrutturato S. Andrea delle Dame, Via L. De Crecchio, 7-80138 Napoli, ¶Istituto di Biostrutture e Bioimmagini, Consiglio Nazionale delle Ricerche, Via Mezzocannone 6, 80134 Napoli, and **Dipartimento di Biologia Strutturale e Funzionale, Università "Federico II," Via Cynthia, 80126 Napoli, Italy*

Onconase (ONC), a member of the RNase A superfamily extracted from oocytes of *Rana pipiens*, is an effective cancer killer. It is currently used in treatment of various forms of cancer. ONC antitumor properties depend on its ribonucleolytic activity that is low in comparison with other members of the superfamily. The most damaging side effect from Onconase treatment is renal toxicity, which seems to be caused by the unusual stability of the enzyme. Therefore, mutants with reduced thermal stability and/or increased catalytic activity may have significant implications for human cancer chemotherapy. In this context, we have determined the crystal structures of two Onconase mutants (M23L-ONC and C87S,des103–104-ONC) and performed molecular dynamic simulations of ONC and C87S,des103–104-ONC with the aim of explaining on structural grounds the modifications of the activity and thermal stability of the mutants. The results also provide the molecular bases to explain the lower catalytic activity of Onconase compared with RNase A and the unusually high thermal stability of the amphibian enzyme.

Ribonucleases are widely found in living organisms and have been proposed to function in RNA metabolism and gene expression (1). Several ribonucleases have been isolated from organs of various animals and have been well characterized. Bovine pancreatic ribonuclease (RNase A)[1] is the most studied member of the family (2). It has been used as a model for the study of the fundamental aspects of protein structure and function (2, 3). Several members of the RNase A superfamily exhibit additional biological functions in connection with their intrinsic ribonucleolytic activities (4, 5). In humans, eosinophil-derived neurotoxin and eosinophil cationic protein (6) exert neurotoxicity as well as antiparasitic activity (7). Bovine seminal ribonuclease (BS-RNase) has been found to induce apoptosis of human thyroid carcinoma cell lines (8, 9). Onconase (ONC) from *Rana pipiens* is cytotoxic (10) and cytostatic to several tumor lines and is currently in phase III clinical trials for the treatment of malignant mesothelioma (8, 11, 12).

ONC shares 30% of identity with the sequence of RNase A, and its three-dimensional structure exhibits a highly conserved ribonuclease-like topology (13), which comprises a characteristic V-shaped β-sheet motif surrounded by three α-helices. Differences are mainly localized in the loop regions, which are significantly shorter in ONC, and at the C terminus where a disulfide bond, unique to amphibian ribonucleases, tethers the C-terminal residue Cys^{104} to Cys^{87} located in one strand of the β-sheet (13). Another distinct property of ONC is the presence of an N-terminal pyroglutamate (Pyr^1), which folds back against the N-terminal helix (13). The overall active site architecture closely resembles that of RNase A and includes His^{10}, Lys^{31}, and His^{97}, which form the catalytic triad corresponding to His^{12}, Lys^{41}, and His^{119}, respectively, of the pancreatic enzyme. Despite this similarity and the activating effect of the N-terminal Pyr residue (14), the Onconase activity is by 3–5 orders of magnitude lower in comparison with RNase A, depending on the used substrate (15). The structural reasons for this very low ribonucleolytic activity are not yet clearly understood.

Although very low, the activity is essential for the Onconase antitumor action (7), which seems to be related to its ability to evade the ribonuclease inhibitor (10), a protein present in human cells that protects them from the potentially damaging effects of their own RNases. Although ONC is a frog protein, it is immunologically tolerated by humans. It only causes a reversible renal toxicity (16), probably linked to the enzyme stability, which is unusually high for a protein isolated from a mesophilic source (17). ONC has a denaturation temperature (T_d) close to 90 °C at pH 6.0 and is particularly resistant to proteolysis (17).

To improve the performance of the protein as an antitumor agent, ONC mutants have been prepared. These mutants were

* This work was supported by research grants Regione Campania "Legge 5" and by an FIRB grant from the Italian Ministero dell'Istruzione e dell'Università. The costs of publication of this article were defrayed in part by the payment of page charges. This article must therefore be hereby marked "*advertisement*" in accordance with 18 U.S.C. Section 1734 solely to indicate this fact.

The atomic coordinates and structure factors (codes 1YV4, 1YV6, and 1YV7) have been deposited in the Protein Data Bank, Research Collaboratory for Structural Bioinformatics, Rutgers University, New Brunswick, NJ (http://www.rcsb.org/).

‖ To whom correspondence may be addressed: Dipartimento di Chimica, Università di Napoli "Federico II" Complesso Universitario di Monte Sant' Angelo, Via Cynthia, 80126 Napoli, Italy. Fax: 39-081-674090; E-mail: lelio.mazzarella@unina.it.

‡‡ To whom correspondence may be addressed: Dipartimento di Chimica, Università di Napoli "Federico II" Complesso Universitario di Monte Sant' Angelo, Via Cynthia, 80126 Napoli, Italy. Fax: 39-081-674090; E-mail: filomena.sica@unina.it.

[1] The abbreviations used are: RNase A, bovine pancreatic ribonuclease; BS-RNase, bovine seminal ribonuclease; dCpdA, 2′-deoxycytidylyl-(3′–5′)-2′deoxyadenosine; MD, molecular dynamic; ONC, Onconase; r.m.s.d., root mean square deviation; (C87S,des104)-ONC, mutant of Onconase with serine replacing cysteine at position 87 and with deletion of Cys^{104}; (C87S,des103–104)-ONC, mutant of Onconase with serine replacing cysteine at position 87 and with deletion of Ser^{103} and Cys^{104}; M23L-ONC, mutant of Onconase with leucine replacing methionine at position 23; RMSIP, root mean square inner product; Pyr, pyroglutamate.

TABLE I
Crystal parameters and data collection statistics

Values in parentheses correspond to the highest resolution shells (1.94–1.90, 1.82–1.78, and 1.54–1.51 Å for (C87S,des103–104)-ONC and room temperature and 100 K temperature structures of M23L-ONC, respectively).

	(C87S,des103–104)-ONC	M23L-ONC	M23L-ONC
T (K)	298	298	100
Space group	$P2_12_12_1$	$P2_12_12_1$	$P2_12_12_1$
a (Å)	32.51	32.54	32.29
b (Å)	41.26	40.88	38.54
c (Å)	69.60	69.41	69.08
Resolution limits (Å)	20.00–1.90	20.00–1.78	20.00–1.51
No. of observations	43,004	46,120	181,712
No. of unique reflections	7,322	8,880	14,146
Completeness (%)	93.5 (92.8)	94.8 (87.2)	99.8 (99.9)
$I/\sigma(I)$	19 (8)	23 (8)	54 (26)
R-merge (%)	6.6 (17.7)	8.0 (18.9)	3.5 (6.6)

proved to have a reduced thermal stability and/or increased catalytic activity (17–19). In particular, the mutant in which methionine 23 has been replaced by leucine (M23L-ONC) is 5-fold more active than the native enzyme and fully toxic toward tumor cells (17). On the other hand, mutants in which the disulfide bond Cys^{87}-Cys^{104} has been eliminated, (C87S,des104)-ONC and (C87S,des103–104)-ONC, exhibit a greatly reduced thermal stability with a T_d of 70.2 and 69.3 °C, respectively (19), whereas their catalytic action and antitumor activity are practically unaffected.

Here we report the crystal structures of (C87S,des103–104)-ONC and M23L-ONC and molecular dynamic (MD) simulations of ONC and (C87S,des103–104)-ONC. The results provide strong evidence of the high rigidity of the enzyme. In particular, despite the strict similarity in the β-sheet architecture, ONC does not possess the β-sheet breathing motion characteristic of RNase A and considered to be functionally important (20–22). The decreased flexibility provides a basis to explain the low affinity of ONC toward nucleotides (23) and, more generally, its lower catalytic activity. It also provides a basis to rationalize the substitution effects on the activity and thermal stability of the mutants.

EXPERIMENTAL PROCEDURES

Crystallization and Data Collection—Mutants of Onconase were expressed in *Escherichia coli* and purified as described previously (17–19). Crystallization was achieved by the sitting-drop vapor-diffusion technique at 277 and 293 K for (C87S,des103–104)-ONC and M23L-ONC, respectively. A volume of 2 μl of protein at 15 mg/ml was mixed with an equal amount of the reservoir solution containing 0.1 M sodium acetate, pH 4.5–4.7, 0.2 M lithium sulfate, and 25–27% (w/v) polyethylene glycol 8000. Crystals of the two mutants grow in 2–4 days; they are nearly isomorphous and belong to the orthorhombic space group $P2_12_12_1$. Diffraction data were collected at room temperature on a ENRAF-NONIUS DIP area detector equipped with an FR591 rotating anode of the Istituto di Biostrutture e Bioimmagini (Consiglio Nazionale delle Ricerche, Naples, Italy). For M23L-ONC, diffraction data were collected also at 100 K on the x-ray diffraction beamline at Elettra Synchrotron, Trieste, Italy. Trehalose (300 mg/ml) was used as cryoprotectant. All data were processed using DENZO and SCALEPACK (24). Crystal parameters and data collection statistics are presented in Table I.

Refinement—The crystal structure of the two mutants was obtained by the nearly isomorphous wild type structure solved by Mosimann and co-workers (13) at 1.7-Å resolution. The refinement was carried out with the program CNS (25). Several alternating cycles of positional refinement, energy minimization, individual temperature factor refinement, and manual model building were performed. Water molecules were inserted into the model at positions corresponding to peaks in the $F_o - F_c$ electron density map with heights greater than 3σ and at hydrogen bonding distances from appropriate atoms. Sulfate anions were also located in difference Fourier maps and added to the current models. The program PROCHECK (26) was used to analyze the quality of the final structures. The refinement statistics are presented in Table II. The figures were drawn using MOLSCRIPT (27) and BOBSCRIPT (28).

Molecular Dynamic Simulations—All MD simulations were performed with GROMACS program (29) using a procedure successfully used for other members of pancreatic-like superfamily (22, 30, 31). Briefly the x-ray structures were immersed in cubic boxes containing more than 6700 water molecules. The ionization state was set to mimic a neutral pH environment. The overall charge of the systems was neutralized by adding the appropriate number of ions more than 7 Å away from the protein surface. The solvent was relaxed by energy minimization followed by a 20-ps MD simulation at 300 K. The overall system was then minimized without restraints before the productive run. All bond lengths were constrained by LINCS (32); Newton's equations of motion were integrated with a time step of 2 fs, and atomic coordinates were saved for analyses every 0.5 ps. A dielectric constant of 1 was used. The simulated temperatures, 300 and 350 K, were kept constant by coupling the system to an external bath (33). A cut-off of 14 Å was used for the treatment of both electrostatic and Lennard-Jones interactions. 4-ns simulations were performed at 300 and 350 K for ONC and for the mutant (C87S,des103–104)-ONC. A second independent 10-ns simulation of ONC was carried out at 300 K using the same parameters of 4-ns simulation but a different set of initial velocities. A brief summary of the simulation procedure is reported in Table III.

Analysis of the MD Trajectories—The global structural stability of the simulations has been evaluated by following several geometric parameters as a function of time. The ONC and (C87S,des103–104)-ONC simulations were stable and exhibited great similarity to the x-ray starting structures at 300 K. The root mean square deviation (r.m.s.d.) values for the Cα atoms are on average 2.2 Å, and the average values for radius of gyration and solvent-accessible surface area are comparable with those experimentally observed. At 350 K, the r.m.s.d. values are 2.2 Å for ONC and 3.2 Å for (C87S,des103–104)-ONC. The mobility of each Cα atom with respect to the average structure (root mean square fluctuation) has been calculated according to Equation 1,

$$\sqrt{\frac{1}{N}\sum_{i=1}^{n}(r_i - \langle r\rangle)^2} \qquad \text{(Eq. 1)}$$

where r_i represents the element position at time i, and r represents the average value.

Essential degrees of freedom were extracted from the equilibrated portions of the trajectories according to the essential dynamic method (34). The eigenvectors corresponding to the higher 10 eigenvalues obtained from diagonalization of the covariance matrix of Cα atom fluctuations were used to describe almost all the conformational substates accessible to the protein (essential subspace). To evaluate the overlap of the conformation spaces spanned by the different systems, we have calculated the root mean square inner product (RMSIP) (22, 35–37).

The RMSIP is defined according to Equation 2,

$$\sqrt{\frac{1}{10}\sum_{i=1}^{10}\sum_{j=1}^{10}(\eta_i\eta_j)^2} \qquad \text{(Eq. 2)}$$

where η_i and η_j are the ith and jth eigenvectors from the two trajectories, respectively. The RMSIP value was also used to ascertain the convergence in the essential subspace between two halves of the equilibrated portion of the trajectories and to evaluate their similarity.

RESULTS AND DISCUSSION

X-ray Structure of M23L-ONC and (C87S,des103–104)-ONC—The room temperature structure of M23L-ONC was re-

TABLE II
Refinement statistics

	(C87S,des103–104)-ONC	M23L-ONC	M23L-ONC
Resolution range (Å)	20.0–1.90	20–1.78	20–1.51
Number of reflections ($F > 2\sigma(F)$)	6,841	8,167	14,085
R-factor/R-free (%)	14.4/19.4	16.8/21.2	15.6/19.8
Number of protein atoms	867[a]	831[a]	826
Water sites	99	90	144
Sulfate anions	1	1	3
r.m.s.d. from stereochemical target values			
Bond length (Å)	0.032	0.007	0.034
Bond angles (°)	2.30	1.53	2.71
Dihedral angles (°)	25.1	24.9	25.3
Improper angles(°)	1.59	0.87	2.08
Average B-factor (Å^2)			
Protein, overall	19.9	17.5	11.2
Main chain	15.6	13.8	7.6
Side chain	20.3	18.4	11.3
Ion atoms	32.0	29.1	24.4
Solvent atoms	36.0	30.2	20.1

[a] The different number of atoms is due to the presence of multiple side chain conformations.

TABLE III
Summary of the MD runs

	ONC	(C87S,des103–104)-ONC
Software used	GROMACS	GROMACS
Starting model (Protein Data Bank code)	1ONC	Present structure
Time (ps)	4,000[a]	4,000
Total number of atoms	20,958	20,896
Number of water molecules	6,732	6,744
Box volume (nm^3)	216	216
Electrostatic interaction treatment	Cut-off truncation method	Cut-off truncation method
Cut-off for Coulombic interactions (Å)	14	14
Cut-off for Lennard-Jones interactions (Å)	14	14
Integration time step (ps)	0.002	0.002
Constraints	LINCS algorithm	LINCS algorithm
Temperature (K)	300 and 350	300 and 350

[a] A second independent 10-ns simulation of ONC was carried out at 300 K using the same parameters of 4-ns simulation but a different set of initial velocities.

fined to an R-factor of 0.168 (R-free = 0.212) using data collected at 1.78-Å resolution and includes 90 water molecules and one sulfate anion. A low temperature model was also obtained by using the 1.51-Å resolution data, collected at 100 K, and refined to a final R-factor of 0.156 (R-free = 0.198); in this case 144 water molecules and three sulfate anions were included in the final model. The room temperature crystal structure of (C87S,des103–104)-ONC, refined at 1.90-Å resolution to a final R-factor of 0.144 (R-free = 0.194), includes 99 water molecules and one sulfate anion. The average B-factors for all the non-hydrogen atoms are 17.5, 11.2, and 19.9 Å^2 for the three structures, respectively. A full list of the refinement statistics is reported in Table II. Fig. 1 gives a general view of the molecule; the mutated and/or deleted residues are *shaded*.

The overall structures of the two mutants, refined with the room temperature data, are very close to that of the wild type enzyme (13), showing that in both cases the mutations do not produce any relevant alteration of the protein tertiary structure. Indeed, after superimposition of each mutant on the native protein, the r.m.s.d. of all the backbone atoms (N, Cα, C, and O) is 0.16 Å for M23L-ONC and 0.13 Å for (C87S,des103–104)-ONC. Slightly higher values were obtained when the 100 K structure of M23L-ONC was compared with the room temperature structure (0.31 Å) or with the wild type enzyme (0.38 Å). The former value is very close to the one obtained when two crystal structures of RNase A, refined at 98 and 300 K, respectively, are compared (38).

The close similarity of the two mutants with the wild type enzyme also extends to the active site region where a sulfate anion is located. This anion, which mimics the phosphate of the natural substrate, hydrogen bonds His^{10} and His^{97} as found in

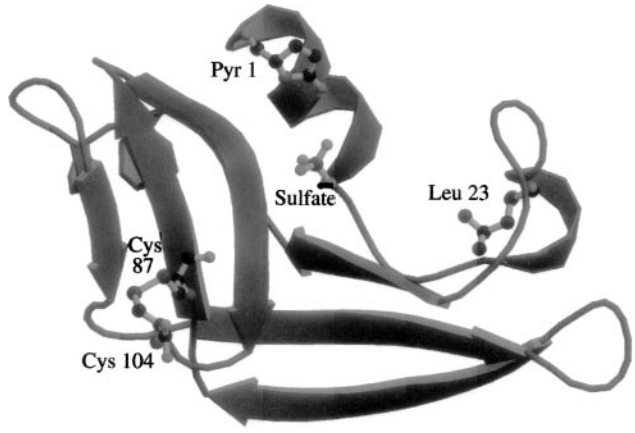

FIG. 1. **A ribbon diagram showing the secondary structural elements in M23L-ONC.** The side chains of Pyr^1 and Leu^{23}, the C-terminal disulfide bridge (Cys^{87}-Cys^{104}), and the active site sulfate ion are drawn in *ball-and-stick* representation.

the structure of the wild type enzyme (13) as well as in several other members of the pancreatic-like superfamily (39–43). In the mutants, as well as in the wild type structure, His^{97} adopts a g^- conformation ($\chi_1 = -76 \pm 3°$) very similar to the B conformation of the corresponding His^{119} in RNase A (44). In this enzyme, His^{119} has access to more than one conformation, although the A conformation (χ_1 close to 180°), which is considered to be catalytically relevant in the transphosphorolytic step, is more often encountered due to the stabilizing interaction with the carboxylate group of Asp^{121} (40). In the corresponding position 99 of Onconase, the presence of a valine

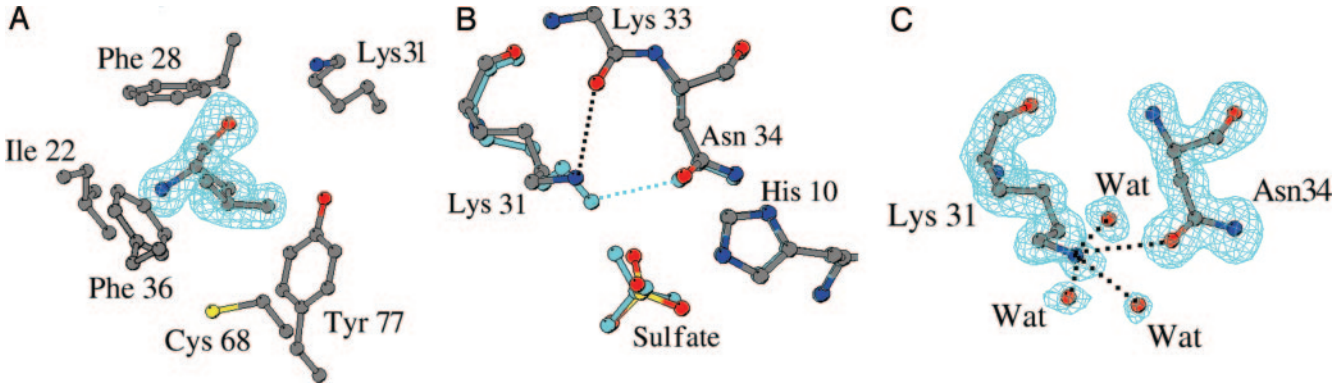

FIG. 2. *A*, hydrophobic cavity surrounding the Leu[23] side chain whose omit $F_o - F_c$ map is contoured at $2\sigma(I)$. *B*, superimposition of the active site region of (C87S,des103–104)-ONC and M23L-ONC (*cyan*) at room temperature. The side chain of Lys[33] was not drawn. *C*, active site architecture in the M23L-ONC structure at 100 K. Hydrogen bonds are represented by *dotted lines*. *Wat*, water.

instead of the aspartate decreases the A conformation stability because of the loss of the salt bridge and the greater steric hindrance of the side chain. This feature is expected to reduce the activity of the enzyme at most in the first step of the enzymatic reaction and cannot account for the dramatic decrease observed for the first as well as for the second rate-limiting hydrolytic step (15). In this context, the explanation of the increased activity of M23L-ONC in comparison with the wild type enzyme on the basis of their structural differences may shed light on the origin of the very low ribonucleolytic activity of Onconase.

In the room temperature model of M23L-ONC, despite its similarity with the wild type enzyme, small conformational changes of residues near the mutation site and in the active site are indeed observed. The side chain of the mutated residue is located in a hydrophobic cavity lined by the side chains of Ile[22], Phe[28], Phe[36], Tyr[77], Cys[68], and Lys[31] and stiffened by the presence of the three aromatic residues (Fig. 2*A*). The greater bulkiness of the Leu branched side chain compared with Met produces a small but significant rearrangement of the contacting residues such as Phe[36] and, particularly, Lys[31], a residue that plays an important role in the ribonucleolytic activity of the enzyme (23). As a consequence, the Nζ of this lysine modifies its hydrogen bonding network. Both in ONC and in (C87S,des103–104)-ONC, the cationic head of Lys[31] is hydrogen-bonded at a distance of 2.9 and 3.2 Å, respectively, to the carbonyl oxygen of Lys[33]. In M23L-ONC, Nζ moves about 0.5 Å away from this oxygen in the direction of the sulfate and establishes an hydrogen bond to Oδ-1 of Asn[34] at a distance of 3.0 Å (4.0 Å in ONC and 3.7 Å in (C87S,des103–104)-ONC) (Fig. 2*B*). Although small, this movement places the side chain in a more favorable position to activate the enzymatic reaction. Incidentally a similar hydrogen bond was found in RNase A between the conserved active site residues Lys[41] and Asn[44] (41). The features observed in the room temperature structure of M23L-ONC were fully confirmed by the 100 K structure refined at a resolution of 1.5 Å. Despite some differences arising from the binding of two extra sulfate anions and the rearrangement of a few exposed side chains, the lysine is practically unmoved and well defined in the electron density map together with its hydration sphere. In this case, in addition to the hydrogen bond to O-δ1 of Asn[34] (3.2 Å), Nζ is bonded to two water molecules in a roughly tetrahedral fashion, whereas its distance from the oxygen of Lys[33] is 3.7 Å (Fig. 2*C*).

A reorientation of the lysine side chain in comparison with the wild type enzyme has been recently detected in a NMR study of a variant of ONC, which, in addition to the replacement of Met[23] with Leu, presents at the N terminus the substitution of Pyr[1] with the sequence Met-Gln (45). It is gratifying to notice that both solid state and solution data converge in the indication that the leucine side chain perturbs the lysine native conformation, thus strengthening the indication that this is a genuine feature of the mutant. A similar subtle modification of the side chain conformation of the catalytic Lys[41] was observed in RNase A and was suggested to be important in the substrate binding (41) and in the pH modulation of the enzyme activity (40, 46). In the same enzyme a very subtle shift of the active site His[119] was considered to affect the catalytic activity of some mutants of the pancreatic enzyme (47).

The elevated stiffness of the Onconase structure can be more deeply appreciated in light of the (C87S,des103–104)-ONC structure. In this mutant, not only the active site region but also the C terminus, despite the lack of the last two residues and of the terminal disulfide bridge, is extremely close to the wild type enzyme (Fig. 3) at a point that the overall r.m.s.d. on backbone atoms is only 0.13 Å. In particular, as reported above, Lys[31] shares with the wild type enzyme the hydrogen bonding network and its conformation is closer to ONC rather than to M23L-ONC. These findings are in line with the experimental result that (C87S,des103–104)-ONC and ONC have comparable catalytic activity (19). Moreover the structural data also demonstrate that the geometrical requirements for the formation of the disulfide bridge Cys[87]-Cys[104] are fully satisfied by the minimum energy conformation reached in the absence of the covalent constraint. This result is not highly surprising as there are several examples of disulfide-deficient variants of proteins that display only small structural variations compared with the wild type enzyme (48–54). Nevertheless the perfect match of the two strands in the absence of the disulfide can be taken as an indication that the disulfide bridge has been implemented in the Onconase software at the very end of the evolutionary pathway of the molecule when its three-dimensional pattern had already been fully defined. This is also in line with the fact that the C-terminal disulfide bridge is not conserved along the RNase A superfamily and appears rather recently in the phylogenetic pathway (55).

In addition to the sulfate in the active site, two more sulfates are located on the surface of the mutant M23L-ONC at 100 K where they are stabilized by intermolecular contacts. In particular SO_4^{701} forms a hydrogen bond with the Nϵ atom of the Trp[3] and interacts with the Nζ atom of Lys[45] and with three water molecules, two of which interact also with SO_4^{901}. SO_4^{901} is located in a cavity lined by residues 40–42, where the largest variations are observed with respect to the native and room temperature structure, and forms hydrogen bonds with the side chain of Arg[40] and with the main chain nitrogen of Gln[42]. The two sulfates are 6.75 Å apart, and their relative position gains further stabilization by the proximity of the Lys[8] side

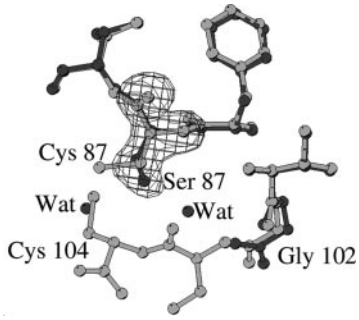

FIG. 3. **C-terminal region of (C87S,des103–104)-ONC (*dark gray*) and ONC (*light gray*; Protein Data Bank code 1ONC) after superimposition.** Two water (*Wat*) molecules take the place of Ser^{103} and Cys^{104} in (C87S,des103–104)-ONC. The omit $F_o - F_c$ map for Ser^{87} is contoured at $2\sigma(I)$.

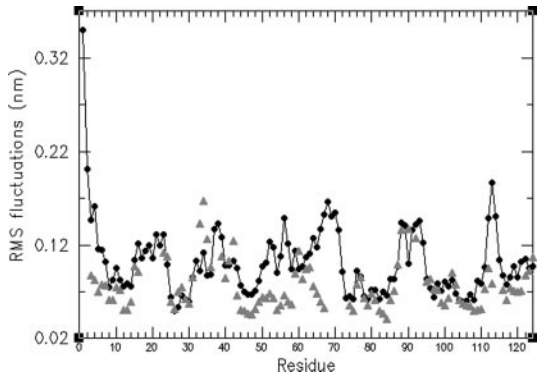

FIG. 4. **Root mean square (*RMS*) fluctuations of Cα atoms in the equilibrated region of the trajectory for ONC (▲) and RNase A (●).** Results of 4-ns molecular dynamic simulation at 300 K are shown.

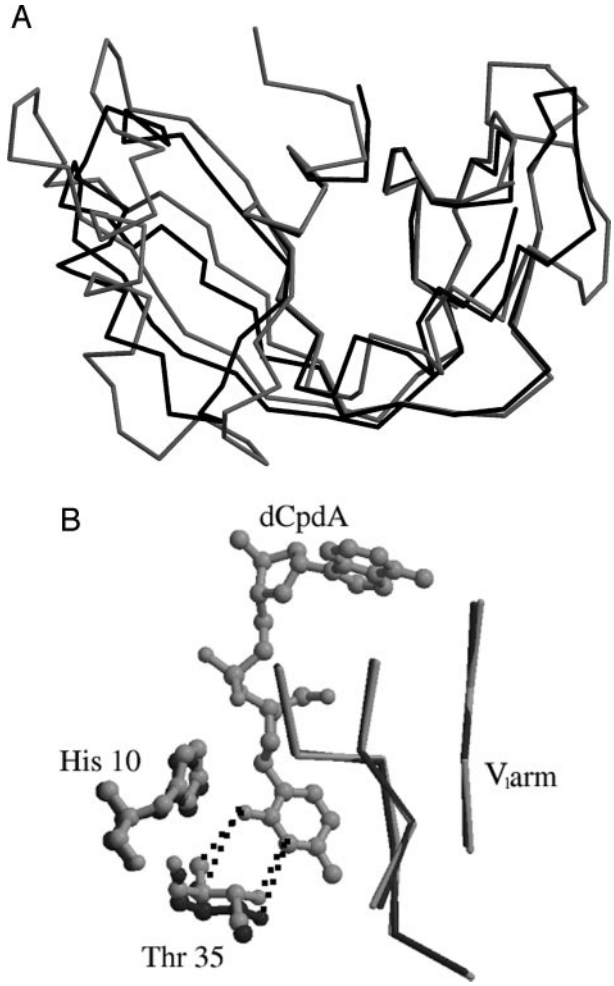

FIG. 5. *A*, Cα atom tracing of ONC structure (*dark gray*) compared with that of RNase A (*light gray*; Protein Data Bank code 1KF2). *B*, superimposition of the complex of RNase A with dCpdA (*light gray*; Protein Data Bank code 1RPG) to ONC (*dark gray*; Protein Data Bank code 1ONC). In both cases the V_1 arm (see text for the definition) was used for the superimposition of the two proteins. Hydrogen bonds are represented by *dotted lines*.

chain of a symmetry-related molecule. Notably the Trp^3 is conserved among the frog ribonucleases, whereas Lys^{45} and residues 40–42 are not. However, the positions of these sulfate anions are considerably different from those of the putative secondary interaction sites, as detected in pancreatic-like ribonucleases (56, 57), and presumably do not have any significant functional role.

MD Simulations of ONC—Enzymatic properties of RNase A have been suggested to be directly correlated to the dynamics of the protein (21, 58) and in particular to a subtle but well documented breathing motion of the β-sheet motif (21). Moreover the low frequency motion can be evidenced by means of molecular dynamic calculations as shown by the results on RNase A (20), on its swapped dimeric forms (30, 31), and on Angiogenin (22), another member of the RNase superfamily.

We have now extended the MD simulations to ONC. The results show that the dynamic behavior of ONC is considerably different from that observed for other RNases. The root mean square fluctuations of Cα atoms are reported in Fig. 4 in comparison with those of RNase A. With the exception of residues 25–28, both regular secondary structure regions (root mean square fluctuation, $\ll$1 Å) and loop residues (root mean square fluctuation, $<$1.7 Å) show lower mobility during the simulation than the structurally aligned residues of RNase A or Angiogenin (data not shown). Moreover none of the first eigenvectors obtained by essential dynamics are suggestive of a collective motion that would resemble the β-sheet motion discussed above. In all previous cases the molecular breathing motion could be detected as one of the highest eigenvectors extracted by 3- or 4-ns trajectories. Nevertheless we have repeated and extended the ONC simulation up to 10 ns with results that match well those obtained in the shorter simulation. Indeed the essential subspaces sampled by ONC in the two trajectories are highly overlapped as indicated by the high value (0.73) of the RMSIP (see "Experimental Procedures" for details). Given the similarity in the results of the two simulations and for sake of homogeneity with the other simulations, only the 4-ns results will be considered further.

The trace of covariance matrix of 0.62 nm^2, calculated in the last 2 ns of the ONC trajectory, is significantly smaller than that calculated from the RNase A simulation (1.30 nm^2) and is comparable to that observed, for instance, for the hyperthermophilic enzymes Sso7d (59) and for rubredoxin from *Pyrococcus furiosus* (60) at room temperature. The elevated rigidity of ONC that emerges from the MD calculations is in a good agreement with the NMR data on the E1S mutant of ONC published by Gorbatyuk *et al.* (45). Their model free analysis of the backbone amide nuclear Overhauser effect relaxation data shows that this molecule exhibits an extremely limited flexibility on the ps/ns time scale with a mean value for the generalized order parameter of 0.94 ± 0.04 and that the active site residues display no distinctive backbone flexibility.

The dynamic features of ONC are of particular interest in relation to the geometry of the active site as it emerges from the published structure of the native enzyme (13) and that of the two mutants presented in this study. The separate superimpo-

sition of the N, Cα, C, and O atoms of the two arms V_1 (residues 55–58, 86–91, and 96–101) and V_2 (residues 33–38, 63–70, and 77–84) of ONC β-sheet on the corresponding regions of RNase A, BS-RNase, and other RNases shows that in comparison the active site cleft between the two arms of the amphibian enzyme β-sheet is significantly wider (Fig. 5*A*). For a more quantitative estimate we have evaluated the distance between the nitrogen amide atoms of Thr^{45} and Phe^{120}, two conservative residues placed on the two arms of the β-sheet, which contribute with two key hydrogen bonds to the stability of the bound substrate in the active site of RNase A (56, 61) and BS-RNase (62, 63). Due to the breathing motion, this distance in the latter proteins depends on several variables, such as crystal packing, crystallization solution, pH, ligands bound to the active site, etc. From a survey of more than 40 RNase A and BS-RNase models in the Protein Data Bank (64), it emerges that the distance spans the interval 7.5–8.5 Å with a mean value of about 8.0 Å. In the Onconase structures the distance between the nitrogen amide atoms of the corresponding residues Thr^{35} and Phe^{98} is sharply restricted to a value close to 9.1 Å. Albeit in the last case the sample is greatly reduced, the distance is significantly larger than the largest value found for the pancreatic and seminal enzymes. As a result, the residues important for catalysis and for the binding of the substrate, such as Lys^{31} and Thr^{35} on the V_2 arm and His^{97} and Phe^{98} on the V_1 arm are about 1 Å further apart in comparison with the corresponding residues of RNase A and BS-RNase. If we use the complex of RNase A with 2′-deoxycytidylyl(3′–5′)-2′deoxyadenosine (dCpdA) (61) as a reference structure, after superimposition of the V_1 arm of ONC with that of the pancreatic enzyme (r.m.s.d. = 0.51 Å) (Fig. 5*B*), the distances of the nitrogen and oxygen atoms of Thr^{35} with N-3C and O-2C atoms of dCpdA are 3.6 and 3.7 Å, respectively. These values are significantly larger than those of the corresponding distances in the complex of the pancreatic enzyme (2.8 and 2.6 Å, respectively) where these hydrogen bonding interactions substantially contribute to the stability of the complex. After the superimposition of V_1, the best superimposition of V_2 requires a further rotation of 5.6°, which decreases the r.m.s.d. between the two V_2 arms from 1.54 to 0.55 Å. Very similar figures are found when the complex of BS-RNase with uridylyl(2′,5′)adenosine (62) is used as a comparison.

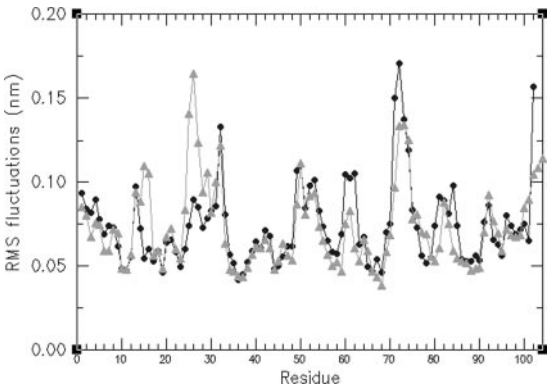

FIG. 6. **Root mean square (*RMS*) fluctuations of Cα atoms in the equilibrated region of the trajectory for ONC (●) and (C87S,des103–104)-ONC (▲) at 300 K.**

This geometric analysis suggests that an efficient binding of the substrate to ONC should require a closure of the two arms similar to the β-sheet breathing motion of RNase A. However, this kind of motion does not appear to be a feature of the Onconase dynamic behavior. Thus, the larger active site cleft, coupled to the unusual low flexibility and in particular to the absence of the breathing motion of the β-sheet, seems to provide a rationale for the low affinity of ONC for its substrate (23) and may be crucial in determining its low catalytic activity.

MD Simulations of (C87S,des103–104)-ONC—Molecular dynamic simulations have been carried out at 300 K for the mutant (C87S,des103–104)-ONC too. The results show a strict similarity with the dynamic behavior of the native protein. Indeed the root mean square deviations of the Cα atoms from the corresponding x-ray structures (2.2 Å) are comparable in the two cases as indeed are the local motions (Fig. 6). Only minor differences can be detected for residues 25–29, which are more mobile in the wild type enzyme, and for residues 72, 73, and 102 that are more flexible in (C87S,des103–104)-ONC. Similarly global motions of the two proteins are analogous as judged by the high RMSIP value (0.70; see "Experimental Procedures" for details) and by the fact that they have the same value of the trace of the covariance matrix (0.62 nm^2).

In conclusion, ONC and (C87S,des103–104)-ONC exhibit almost identical structures and identical dynamic behavior on the ps/ns time scale at 300 K. These findings demonstrate that the (C87S,des103–104)-ONC is as rigid as ONC and that the low flexibility of the amphibian enzyme cannot be related to the presence of the C-terminal disulfide bridge. On the other hand, the two proteins do show a marked difference in thermal stability and do show a different behavior when the MD simulations were performed at higher temperature.

MD Simulations at 350 K—MD simulations have been carried out at 350 K for both ONC and (C87S,des103–104)-ONC. High temperature simulations have been increasingly performed in the last few years to detect the first steps of the unfolding pathway of proteins (65, 66) and to address features of protein thermal stability (59, 60, 67). At this temperature the root mean square deviations of the Cα atoms from the starting

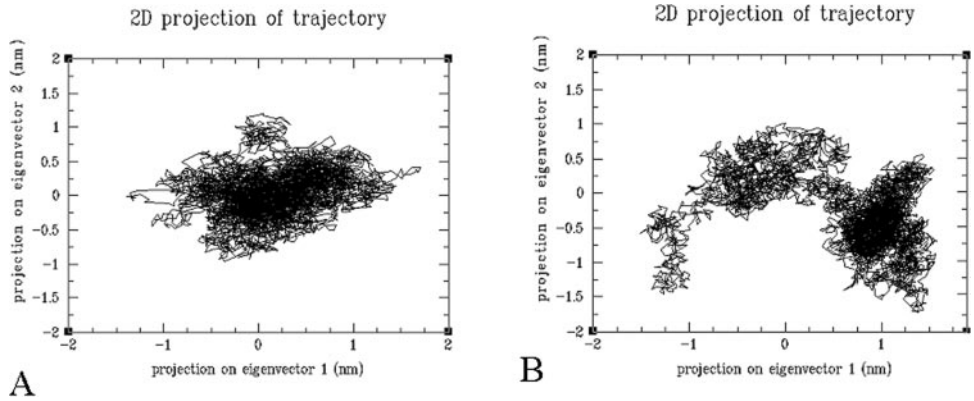

FIG. 7. **Projection of the Cα atom trajectory along the first two eigenvectors derived from the essential dynamic analysis for ONC (*A*) and (C87S,des103–104)-ONC (*B*) at 350 K.** *2D*, two-dimensional.

x-ray structures for (C87S,des103–104)-ONC are significantly higher than the value obtained for ONC at the same temperature (3.2 *versus* 2.2 Å). The traces of the covariance matrices are also different (1.20 *versus* 0.79 nm^2), supporting the conclusion that the higher temperature of the simulation is sufficient to alter the amplitude of the fluctuations in (C87S,des103–104)-ONC but not in ONC. Indeed the main difference between the two proteins, as revealed by the simulations, is the finding that ONC samples similar essential subspaces at 300 and 350 K (RMSIP, 0.69), whereas the conformational subspaces sampled by (C87S,des103–104)-ONC at the studied temperatures are much less overlapped (RMSIP, 0.55). Interestingly similar results were obtained when comparing the dynamics of the hyperthermophilic protein Sso7d and its truncated and less stable variant at two different temperatures (59). To show the dynamic differences between ONC and (C87S,des103–104)-ONC at 350 K in terms of conformational space sampling, the projection of the Cα atom trajectory along the first two eigenvectors derived from the essential dynamic analysis for ONC and (C87S,des103–104)-ONC is reported in Fig. 7, *A* and *B*. The figure clearly shows that at 350 K (C87S,des103–104)-ONC samples a larger conformational space compared with ONC. This difference is clearly triggered by the absence of the C-terminal disulfide bridge, and its reduced thermal stability compared with ONC has to be attributed to the greatly increased number of conformations accessible to the unfolded state.

CONCLUSIONS

Our present and previous (17, 45) results clearly indicate two distinctive features of Onconase with respect to other ribonucleases: very small flexibility and very high thermal stability, both unusual properties for a mesophilic enzyme. The two properties are mainly governed by different structural features. Rigidity is in principle related to small (harmonic) atomic positional displacements close to the equilibrium conformation and is controlled by the second derivative at the equilibrium position of the potential constraining the equilibrium structure. By contrast the energetic features of larger anharmonic displacements must play an important role in determining the resistance of the molecule to unfold.

In Onconase the molecular features controlling these two properties of the enzyme are in a first place orthogonal. Structural and dynamic properties of (C87S,des103–104)-ONC clearly indicate that the loss of the C-terminal disulfide bridge does not affect the rigidity of the enzyme; however, it dramatically reduces the protein thermal stability by increasing the conformational space accessible to the protein at high temperature as suggested by the 350 K MD simulations. By contrast, the origin of the low flexibility of the β-sheet region of ONC is probably connected to the reduced length of the loops between the secondary structure elements. In this respect, the enzyme can be considered an essential ribonuclease that maintains intact the regular structure regions of the ribonuclease folding but has reduced *at minimum* all the exposed connecting loops. This feature can be effective in forcing the V-shaped β-sheet to adopt a more opened structure with respect to RNase A. Thus, the larger cleft coupled with the unusually low flexibility of the β-sheet region may be at the origin of the low affinity of the enzyme for the substrate (23) and of the low ribonucleolytic activity. Interestingly all amphibian ribonucleases (RC-RNase 2, RC-RNase 4, and ONC) that lack the loop following the second helix in RNases (residues 35–40 in RNase A) show very low catalytic activity comparable to that of ONC. In a rigid enzyme, as ONC is, the induced fit can be partially inhibited, and therefore, significant alterations of the function can be obtained even by very subtle variations of the side chains of catalytically important residues. In this respect the M23L-ONC mutant is highly emblematic: the mutation produces a slight modification of the catalytic residue Lys^{31}, and this *less than 1.0-Å change* (68) in the position of Nζ can well account for the significant increase of the mutant catalytic activity. The finding that for Onconase very small changes significantly perturb the catalytic activity can be used to obtain a fine tuning of ONC properties and improved antitumor drugs.

Acknowledgments—We are grateful to Giosuè Sorrentino and Maurizio Amendola for technical assistance and to Elettra Trieste for providing synchrotron radiation facilities.

REFERENCES

1. D'Alessio, G. (1993) *Trends Cell Biol.* **3,** 106–109
2. Raines, R. T. (1998) *Chem. Rev.* **98,** 1045–1066
3. Blackburn, P., and Moore, S. (1982) in *The enzymes* (Boyer, P. D., ed) pp. 317–433, Academic Press, New York
4. Matousek, J., Soucek, J., Riha, J., Zankel, T. R., and Benner, S. A. (1995) *Comp. Biochem. Physiol. B Biochem. Mol. Biol.* **112,** 235–241
5. Matousek, J. (2001) *Comp. Biochem. Physiol. C Toxicol. Pharmacol.* **129,** 175–191
6. Gleich, G. J., Loegering, D. A., Bell, M. P., Checkel, J. L., Ackerman, S. J., and McKean, D. J. (1986) *Proc. Natl. Acad. Sci. U. S. A.* **83,** 3146–3150
7. Youle, R. J., and D'Alessio, G. (1996) in *Ribonuclease: Structures and Functions* (D'Alessio, G., and Riordan, J. F., eds) pp. 491–514, Academic Press, New York
8. Matousek, J., Soucek, J., Slavik, T., Tomanek, M., Lee, J. E., and Raines, R. T. (2003) *Comp. Biochem. Physiol. C Toxicol. Pharmacol.* **136,** 343–356
9. Soucek, J., Pouckova, P., Matousek, J., Stockbauer, P., Dostal, J., and Zadinova, M. (1996) *Neoplasma* **43,** 335–340
10. Wu, Y., Mikulski, S. M., Ardelt, W., Rybak, S. M., and Youle, R. J. (1993) *J. Biol. Chem.* **268,** 10686–10693
11. Irie, M., Nitta, K., and Nonaka, T. (1998) *Cell. Mol. Life Sci.* **54,** 775–784
12. Makarov, A. A., and Ilinskaya, O. N. (2003) *FEBS Lett.* **540,** 15–20
13. Mosimann, S. C., Ardelt, W., and James, M. N. (1994) *J. Mol. Biol.* **236,** 1141–1153
14. Newton, D. L., Boque, L., Wlodawer, A., Huang, C. Y., and Rybak, S. M. (1998) *Biochemistry* **37,** 5173–5183
15. Boix, E., Wu, Y., Vasandani, V. M., Saxena, S. K., Ardelt, W., Ladner, J., and Youle, R. J. (1996) *J. Mol. Biol.* **257,** 992–1007
16. Vasandani, V. M., Burris, J. A., and Sung, C. (1999) *Cancer Chemother. Pharmacol.* **44,** 164–169
17. Notomista, E., Catanzano, F., Graziano, G., Dal Piaz, F., Barone, G., D'Alessio, G., and Di Donato, A. (2000) *Biochemistry* **39,** 8711–8718
18. Notomista, E., Cafaro, V., Fusiello, R., Bracale, A., D'Alessio, G., and Di Donato, A. (1999) *FEBS Lett.* **463,** 211–215
19. Notomista, E., Catanzano, F., Graziano, G., Di Gaetano, S., Barone, G., and Di Donato, A. (2001) *Biochemistry* **40,** 9097–9103
20. Merlino, A., Vitagliano, L., Ceruso, M. A., Di Nola, A., and Mazzarella, L. (2002) *Biopolymers* **65,** 274–283
21. Vitagliano, L., Merlino, A., Zagari, A., and Mazzarella, L. (2002) *Proteins* **46,** 97–104
22. Merlino, A., Vitagliano, L., Ceruso, M. A., and Mazzarella, L. (2003) *Proteins* **53,** 101–110
23. Lee, J. E., and Raines, R. T. (2003) *Biochemistry* **42,** 11443–11450
24. Otwinowsky, Z., and Minor, W. (1997) *Methods Enzymol.* **276,** 307–326
25. Brunger, A. T., Adams, P. D., Clore, G. M., DeLano, W. L., Gros, P., Grosse-Kunstleve, R. W., Jiang, J. S., Kuszewski, J., Nilges, M., Pannu, N. S., Read, R. J., Rice, L. M., Simonson, T., and Warren, G. L. (1998) *Acta Crystallogr. Sect. D Biol. Crystallogr.* **54,** 905–921
26. Laskowski, R. A., MacArthur, M. W., Moss, M. D., and Thorton, J. M. (1993) *J. Appl. Crystallogr.* **26,** 283–291
27. Kraulis, P. J. (1991) *J. Appl. Crystallogr.* **24,** 946–950
28. Esnouf, R. M. (1999) *Acta Crystallogr. Sect. D Biol. Crystallogr.* **55,** 938–940
29. van der Spoel, D., van Druner, R., and Berendsen, H. J. (1994) *GROningen MAchine for Chemical Simulation*, Department of Biophysical Chemistry, BIOSON Research Institute, Groningen, The Netherlands
30. Merlino, A., Vitagliano, L., Ceruso, M. A., and Mazzarella, L. (2004) *Biophys. J.* **86,** 2383–2391
31. Merlino, A., Ceruso, M. A., Vitagliano, L., and Mazzarella, L. (2005) *Biophys. J.* **88,** 2003–2012
32. Hess, B., Bekker, H., Berendsen, H. J., and Freaje, J. G. E. M. (1997) *J. Comp. Chem.* **18,** 1463–1472
33. Berendsen, H. J., Postma, J. P., van Gusteren, W. F., Di Nola, A., and Haak, J. R. (1984) *J. Chem. Phys.* **81,** 3684–3690
34. Amadei, A., Linssen, A. B., and Berendsen, H. J. (1993) *Proteins* **17,** 412–425
35. Ceruso, M. A., Amadei, A., and Di Nola, A. (1999) *Protein Sci.* **8,** 147–160
36. van Aalten, D. M., Conn, D. A., de Groot, B. L., Berendsen, H. J., Findlay, J. B., and Amadei, A. (1997) *Biophys. J.* **73,** 2891–2896
37. de Groot, B. L., Hayward, S., van Aalten, D. M., Amadei, A., and Berendsen, H. J. (1998) *Proteins* **31,** 116–127
38. Tilton, R. F., Jr., Dewan, J. C., and Petsko, G. A. (1992) *Biochemistry* **31,** 2469–2481
39. Mazzarella, L., Capasso, S., Demasi, D., Di Lorenzo, G., Mattia, C. A., and Zagari, A. (1993) *Acta Crystallogr. Sect. D Biol. Crystallogr.* **49,** 389–402
40. Berisio, R., Lamzin, V. S., Sica, F., Wilson, K. S., Zagari, A., and Mazzarella, L. (1999) *J. Mol. Biol.* **292,** 845–854
41. Vitagliano, L., Merlino, A., Zagari, A., and Mazzarella, L. (2000) *Protein Sci.* **9,**

1217–1225
42. Esposito, L., Vitagliano, L., Sica, F., Sorrentino, G., Zagari, A., and Mazzarella, L. (2000) *J. Mol. Biol.* **297,** 713–732
43. Acharya, K. R., Shapiro, R., Allen, S. C., Riordan, J. F., and Vallee, B. L. (1994) *Proc. Natl. Acad. Sci. U. S. A.* **91,** 2915–2919
44. Borkakoti, N., Palmer, R. A., Haneef, I., and Moss, D. S. (1983) *J. Mol. Biol.* **169,** 743–755
45. Gorbatyuk, V. Y., Tsai, C. K., Chang, C. F., and Huang, T. H. (2004) *J. Biol. Chem.* **279,** 5772–5780
46. Berisio, R., Sica, F., Lamzin, V. F., Wilson, K. S., Zagari, A., and Mazzarella, L. (2002) *Acta Crystallogr. Sect. D Biol. Crystallogr.* **58,** 441–450
47. Chatani, E., Hayashi, R., Moriyama, H., and Ueki, T. (2002) *Protein Sci.* **11,** 72–81
48. Vogl, T., Brengelmann, R., Hinz, H. J., Scharf, M., Lotzbeyer, M., and Engels, J. W. (1995) *J. Mol. Biol.* **254,** 481–496
49. Kelley, J. J., III, Caputo, T. M., Eaton, S. F., Laue, T. M., and Bushweller, J. H. (1997) *Biochemistry* **36,** 5029–5044
50. Forman-Kay, J. D., Clore, G. M., Stahl, S. J., and Gronenborn, A. M. (1992) *J. Biomol. NMR* **2,** 431–445
51. Laity, J. H., Lester, C. C., Shimotakahara, S., Zimmerman, D. E., Montelione, G. T., and Scheraga, H. A. (1997) *Biochemistry* **36,** 12683–12699
52. Shimotakahara, S., Rios, C. B., Laity, J. H., Zimmerman, D. E., Scheraga, H. A., and Montelione, G. T. (1997) *Biochemistry* **36,** 6915–6929
53. Kowalski, J. M., Parekh, R. N., and Wittrup, K. D. (1998) *Biochemistry* **37,** 1264–1273
54. Stone, M. J., Chandrasekhar, K., Holmgren, A., Wright, P. E., and Dyson, H. J. (1993) *Biochemistry* **32,** 426–435
55. Beintema, J. J., Schueller, C., Irie, M., and Carsana, A. (1988) *Prog. Biophys. Mol. Biol.* **51,** 165–192
56. Fontecilla-Camps, J. C., de Llorens, R., le Du, M. H., and Cuchillo, C. M. (1994) *J. Biol. Chem.* **269,** 21526–21531
57. Gilliland, G. (1997) in *Ribonuclease: Structures and Functions* (D'Alessio, G., and Riordan, J. F., eds) pp. 306–341, Academic Press, New York
58. Rasmussen, B. F., Stock, A. M., Ringe, D., and Petsko, G. A. (1992) *Nature* **357,** 423–424
59. Merlino, A., Graziano, G., and Mazzarella, L. (2004) *Proteins* **57,** 692–701
60. Grottesi, A., Ceruso, M. A., Colosimo, A., and Di Nola, A. (2002) *Proteins* **46,** 287–294
61. Zegers, I., Maes, D., Dao-Thi, M. H., Poortmans, F., Palmer, R., and Wyns, L. (1994) *Protein Sci.* **3,** 2322–2339
62. Vitagliano, L., Adinolfi, S., Riccio, A., Sica, F., Zagari, A., and Mazzarella, L. (1998) *Protein Sci.* **7,** 1691–1699
63. Merlino, A., Vitagliano, L., Sica, F., Zagari, A., and Mazzarella, L. (2004) *Biopolymers* **73,** 689–695
64. Berman, H. M., Bhat, T. N., Bourne, P. E., Feng, Z., Gilliland, G., Weissig, H., and Westbrook, J. (2000) *Nat. Struct. Biol.* **7,** (suppl.) 957–959
65. Day, R., and Daggett, V. (2003) *Adv. Protein Chem.* **66,** 373–403
66. Daggett, V. (2002) *Acc. Chem. Res.* **35,** 422–429
67. de Bakker, P. I., Hunenberger, P. H., and McCammon, J. A. (1999) *J. Mol. Biol.* **285,** 1811–1830
68. Koshland, D. E., Jr. (1998) *Nat. Med.* **4,** 1112–1114